Identifying the mechanisms and molecular targets of Hongjingtian injection on treatment of TGFβ1-induced HK-2 cells: coupling network pharmacology with experimental verification

Guanghui Sun[1], Mingwen Jiao[2], Yuying Cui[1], Xuezhen Liang[1,3], Xiaodong Liang[4], Shanshan Zhang[1#], Congcong Guo[5,6#]

[1]First Clinical Medical College, Shandong University of Traditional Chinese Medicine, Jinan, China; [2]Department of General Surgery, The First Affiliated Hospital of Shandong First Medical University & Shandong Provincial Qianfoshan Hospital, Jinan, China; [3]Orthopaedic Microsurgery, Affiliated Hospital of Shandong University of Traditional Chinese Medicine, Jinan, China; [4]College of Traditional Chinese Medicine, Shandong University of Traditional Chinese Medicine, Jinan, China; [5]Department of Endocrinology and Metabology, Affiliated Hospital of Shandong University of Traditional Chinese Medicine, Jinan, China; [6]Department of Endocrinology and Metabology, The First Affiliated Hospital of Shandong First Medical University & Shandong Provincial Qianfoshan Hospital, Jinan, China

Contributions: (I) Conception and design: CC Guo, SS Zhang; (II) Administrative support: CC Guo; (III) Provision of study materials or patients: GH Sun, MW Jiao; (IV) Collection and assembly of data: MW Jiao, XZ Liang; (V) Data analysis and interpretation: YY Cui, XD Liang; (VI) Manuscript writing: All authors; (VII) Final approval of manuscript: All authors.

[#]These authors contributed equally to this work and should be considered as co-corresponding author.

Correspondence to: Congcong Guo. Department of Endocrinology and Metabology, The First Affiliated Hospital of Shandong First Medical University & Shandong Provincial Qianfoshan Hospital, Jinan 250000, China. Email: gccqfshospital@163.com. Shanshan Zhang. First Clinical Medical College, Shandong University of Traditional Chinese Medicine, Jinan 250355, China. Email: zss_@163.com.

Background: The study was designed to investigate the mechanism of Hongjingtian injection (HJT) in treating tubulointerstitial fibrosis (TIF) in chronic kidney diseases (CKD) based on network pharmacology and experimental verification.

Methods: First, active ingredients of HJT obtained from literature were screened using the Traditional Chinese Medicine Systems Pharmacology (TCMSP) database and putative targets of active ingredients were predicted using the Chemmapper, SEA and Swiss Target Prediction database. Subsequently, the "compound-target" network for HJT was established. In addition, TIF disease targets were obtained from the GEO gene chips (accession number GSE20247). The intersecting targets of HJT and TIF obtained through Venny 2.1.0. The key targets and signaling pathways were determined by protein-protein interaction (PPI) and Kyoto Encyclopedia of Genes and Genomes (KEGG) analysis. Finally, quantitative polymerase chain reaction (qPCR) and Western blot (WB) were used to validate the predicted five key genes targets (*GAD1*, *SPHK1*, *P4HA2*, *AKR1B1*, *PTGES*). And immunofluorescence, wound healing assay and transwell assay were used to verify the anti-fibrosis effect of HJT on TGFβ1-induced HK-2 cells.

Results: The network pharmacology analysis results showed that there are 36 active compounds and 1,044 putative target genes in HJT. HJT may exert its inhibitory effects against TIF by acting on 79 key targets. Besides, KEGG analysis indicated that the anti-TIF effect of HJT was mediated by multiple pathways, such as the metabolic pathway, pathways in cancer and gap junction. Among them, *GAD1*, *SPHK1*, *P4HA2*, *AKR1B1* and *PTGES* are enriched in the metabolic pathway. *In vitro* induced cell model experiments, the immunofluorescence experience showed that HJT could restore EMT of HK-2 cells. In addition, the qPCR and WB results showed that HJT significantly restored the expression of the *SPHK1* in HK-2 cells induced by TGF-β1.

Conclusions: This study comprehensively illuminated the active compounds, potential targets, and molecular mechanism of HJT against TIF. HJT treatment of TIF may reverse EMT caused by TGF-β1 by targeting *SPHK1*.

Introduction

Tubulointerstitial fibrosis (TIF) is an irreversible organic change of kidney caused by many pathogenic factors (1). TIF characterized by tubular atrophy, the activation of interstitial fibroblasts and extracellular matrix (ECM) accumulation, is the basic pathological process that chronic kidney diseases (CKD) eventually move towards chronic renal failure (2).

However, due to the complex mechanism of TIF, there are no specific preventive and therapeutic measures in clinical practice. So, it is still a hot research topic to seek effective prevention and treatment measures. Traditional Chinese medicine (TCM) therapy is a unique treatment in China, which has significant clinical efficacy and less side effects. In recent years, many studies have confirmed that TCM has become an effective method to treat TIF through a variety of experimental methods (3,4). TCM injection is a therapeutic drug combining TCM theory and modern scientific means. It is made into a finished product by extracting the pharmaceutical compounds of herb-medicine, which has the characteristics of quick onset and rapid action. The Hongjingtian injection (HJT) is a water-soluble extract of Rhodiola. In China, HJT has been used to treat vascular diseases. Clinical studies have shown that HJT can improve hemorheology, reduce intima-media thickness, and alleviate atherosclerotic inflammatory reaction (5,6). Our previous study has demonstrated that salidroside, the main component of HJT, have renoprotective effects to reduce proteinuria, inhibit renal fibrosis (7).

However, elucidating the pharmacological effects of HJT on TIF is challenging, due to the complex active compounds and unclear mechanism of action. Recently, with the growing understanding of complex diseases, the focus of drug mechanism has shifted from the well-accepted "one target, one compound" model designed toward a single target to a new "multi-target, multi-compound" model aimed at systemically modulating multiple targets. Fully understanding the complex network relationships among diseases, targets, and compounds still remains a big challenge. Fortunately, with the rapid development of systems biology, multidirectional pharmacology, computational biology, network pharmacology has become a new paradigm for clarifying the multivariable interactions of compound-gene-disease system. It provides new scientific and technological support for the mechanism of TCM at the system level, and provides new ideas and directions for experimental research of TCM.

Therefore, in this study, we combined the network pharmacology with the Gene Expression Omnibus (GEO) database to further explore and explain the possible mechanism of HJT in treating TIF. Moreover, the potential mechanism and key target were verified by cell experiments. The flowchart is presented in *Figure 1*. We present the following article in accordance with the MDAR reporting checklist (available at https://atm.amegroups.com/article/view/10.21037/atm-22-5035/rc).

Highlight box

Key findings
- The key finding of the study is that Hongjingtian injection (HJT) may reverse the EMT caused by TGF-β1 to treat Tubulointerstitial fibrosis (TIF) by targeting *SPHK1*.

What is known and what is new?
- TIF is an irreversible organic change of kidney caused by many pathogenic factors. TIF is the basic pathological process that chronic kidney diseases (CKD) eventually move towards chronic renal failure.
- This study comprehensively illuminated the active compounds, potential targets, and molecular mechanism of HJT against TIF.

What is the implication, and what should change now?
- HJT may be an effective measure to prevent and treat CKD. It is necessary to conduct further *in vivo* experimental verification of the potential active ingredients in order to clarify the theoretical prediction.
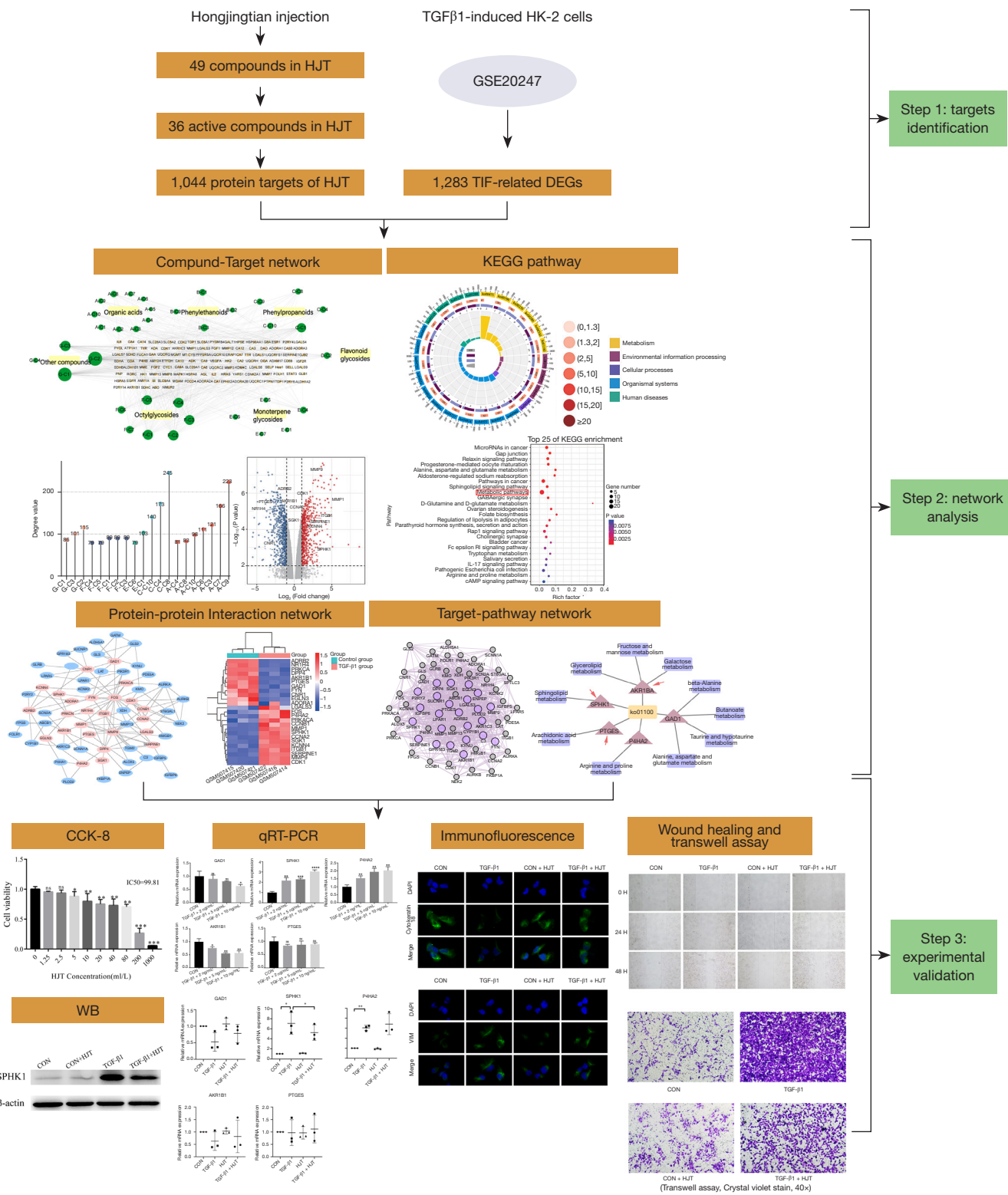
Methods

Screening and identification of active compounds and potential targets of HJT

A total of 49 compounds of HJT were obtained by searching the literature (8). To identify the active compounds of HJT,

Figure 1 The technical strategy of the current study. HJT, Hongjingtian injection; TIF, treating tubulointerstitial fibrosis; DEG, differentially expressed gene; KEGG, Kyoto Encyclopedia of Genes and Genomes; qRT-PCR, quantitative real-time polymerase chain reaction; WB, Western blot.

Page 4 of 23

Sun et al. Mechanisms and targets of HJT on TGFβ1-induced HK-2 cells

the ingredients conforming to the requirements of lipinski, based on the published literature and the information from the SwissADME database (http://www.swissadme.ch/). Subsequently, putative targets of these potential compounds were identified from the ChemMapper (http://lilab.ecust.edu.cn/chemmapper/), Swiss Target Prediction (http://www.swisstargetprediction.ch/) and SEA (http://sea.bkslab.org) database. Then, the UniProt database (https://www.uniprot.org/) was used to convert targets into official gene symbol. Eventually, all putative targets of HJT were retrieved after removing duplicated targets. In addition, Cytoscape 3.7.2 software was used to establish and visualize the compound-target network of HJT based on the obtained results.

Search, identification, and analysis of differentially expressed gene (DEG)

Expression profiling data from GSE20247 were downloaded from the GEO database (http://www.ncbi.nlm.nih.gov/geo/) based on the microarray platform GPL570 (Affymetrix Human Gene Expression Array), which contained 3 samples from healthy individuals and 3 TGF-β1-induced TIF samples. Based on the annotation information in the platform, probe IDs were used to identify the corresponding genes. Genes with an adjusted P<0.01 and log2(fold change) >1 or log2(fold change) <–1 were considered significantly differentially expressed and TIF-related targets. Then, these DEGs were visualized using a volcano plot. The study was conducted in accordance with the Declaration of Helsinki (as revised in 2013).

Enrichment of the Kyoto Encyclopedia of Genes and Genomes (KEGG) pathway

Based on the above analysis, the Venn diagram that intersects the potential targets of HJT and the DEGs of TIF was drawn by Jvenn (http://jvenn.toulouse.inra.fr/app/index.html). Then, with the help of Omicshare information platform (https://www.omicshare.com/), we employed the KEGG pathway analysis the gene related signaling pathway (9).

Construction of protein-protein interaction (PPI) network and key targets analysis

The PPI network of these intersection targets was obtained by using the String online tool (https://string-db.org/) (10) and visualized using the Cytoscape V3.7.2 (https://www.cytoscape.org/). Then, core targets were selected according

to the median values of Degree Centrality (DC), Closeness Centrality (CC), and Betweenness Centrality (BC), which are the three most important parameters for screening the core composite targets (11). Subsequently, the co-expression relationship of genes in the PPI network were analyzed by using the MCODE module in Cytoscape V3.7.2. Ultimately, the key genes enriched in the selected pathway were selected and "key target-signal pathway map" were made using the Cytoscape V3.7.2.

Experimental validation

Reagents and antibodies

TGF-β1 was obtained from novoprotein (CA59, Suzhou, China). HJT was obtained from Tonghua Yusheng Pharmaceutical Co., Ltd. (YBZ11852006, Tonghua, China). Anti-cytokeratin18 was obtained from Boster (A01357-1, Wuhan, China). Anti-Vimentin was obtained from proteintech (10366-1-AP, Wuhan, China). Anti-*SPHK1* was obtained from proteintech (10670-1-AP, Wuhan, China).

Cell culture and treatments

The cell lines HK-2 were obtained from Procell (PC-H2022062701, Wuhan, China). The cells were cultured in modified Eagle's medium (SH30024, MEM, HyClone) with 12% fetal bovine serum (Gibco, Thermo Fisher Scientific, USA) and 1% penicillin-streptomycin (J160016, Hyclone, USA). All cells were maintained in 5% CO_2 at 37 ℃ under a humidified atmosphere. For inducing EMT, cells were treated with different concentrations of TGF-β1 (0, 2, 5 and 10 ng/mL) at 37 ℃ for 48 h.

Cell Counting Kit-8 (CCK8) assay

A total of $3×10^3$ HK-2 cells were plated in 96-well plates and, after a 24 h incubation period, cells were treated with different concentrations of HJT (0, 1.25, 2.5, 5, 10, 20, 40, 80, 200, 1,000 mL/L) at 37 ℃ for 48 h. Subsequently, 10 µL CCK8 solution (A311-02-AA, Vazyme, China) was added to each well and incubated at 37 ℃ for a further 2 h, and cell viability was determined by measuring the absorbance at 450 nm on a spectrophotometer.

Quantitative real-time polymerase chain reaction (qRT-PCR) analysis

Total RNA was extracted using a SPARK easy Cell RNA Kit (AC0205, Sparkjade, China,) and cDNA was

synthesized using a SPARK script II RT Plus Kit (AG0304, Sparkjade, China) according to the manufacturer's protocol. Subsequently, the quality of the extracted RNA was detected. The primer sequences were as follows: *SPHK1* (forward) 5'-CTGTCACCCATGAACCTGCTGTC-3' and (reverse) 5'-ACGCCGATACTTCTCACTCTCTAGG-3', *P4HA2* (forward) 5'-CCAGGAACCAAGTACCAGGCAATG-3' and (reverse) 5'-CTGCTCCATCCACAACACCGTATG-3', *GAD1* (forward) 5'-TCCTCCTGGAAGTGGTGGACATAC-3' and (reverse) 5'-AGCAACTGGTGTGGGTGATGAAAG-3', AKR1B1 (forward) 5'-TGACACCAGAACGCATTGCTGAG-3' and (reverse) 5'-AGACCCTCCAGTTCCTGTTGTAGC-3' and *PTGES* (forward) 5'-TCCTGGGCTTCGTCTACTCCTTTC-3', and (reverse) 5'-TGTAGGTCACGGAGCGGATGG-3' and *GAPDH* (forward) 5'-CCTTCCGTGTCCCCACT-3', and (reverse) 5'-GCCTGCTTCACCACCTTC-3'. Real-time PCR was performed using a SYBR qPCR SuperMix Plus (R311-02, Vazyme, China). The thermocycling conditions were as follows: Initial denaturation at 95 ℃ for 2 min, followed by 40 amplification cycles at 95 ℃ for 15 sec and 60 ℃ for 10 sec. GAPDH was used as the endogenous control for normalization, and the expression was analyzed using the $2^{-\Delta\Delta CT}$ method. The data were extracted from three independent biological experiments with three technical replicates in each experiment.

Western blot (WB) analysis

The total protein in HK-2 cell was collected by RIPA lysis method and the protein concentration was detected by using BCA kit (PC0020, Solarbio, China). Then the proteins were separated using 12% SDS-PAGE (G2037, Servicebio, China) electrophoresis and transferred to PVDF membrane via the electro-blotting at 210 mA for 75 minutes. After taking out the PVDF membrane, wash it three times with TBST for 15 minutes each time. A 5% skimmed milk powder was added and sealed for 2 h. Primary antibody (1:1,000) was put in and cultivated in a refrigerator at 4 ℃ overnight. The next day, TBST was used for washing three times to remove primary antibody, HRP labeled secondary antibody (1:5,000) was added. After incubation for 2 h, TBST was used for washing three times, with 15 min each time. Finally, ECL luminescence kit (E412-02, Vazyme, China) was used for luminescence and the results of WB analysis were performed by using the software ImageJ. The data were extracted from three independent biological

experiments.

Wound healing assay

HK-2 cells at 10^6 cells/mL were cultured in 6-well plate. A 1,000 µL pipette was used to create a scratch in the cells. The non-adherent cells were removed by two washes of PBS, and cells in experimental group were intervened with HJT (2.5 mL/L), TGF-β1 (10 ng/mL) and the TGF-β1 and HJT (10 ng/mL TGF-β1+ 2.5 mL/L HJT). Subsequently, the cells were maintained at 37 ℃ for 48 h. The scratches were photographed at 0, 24 and 48 h respectively by an inverted microscope (XD202, Jiangnan, China). Finally, calculate the relative distance according to the equation $(W_0–W_t)/W_0 \times 100\%$. The data were extracted from three technical replicates.

Transwell assay

10^5 cells/mL of HK-2 after the intervention were collected and inoculated in the upper chamber, and the cells were cultured in serum-free medium for 12 h. The non-invading cells on the upper chamber were eliminated using a cotton swab. After fixing with 4% paraformaldehyde, the cells on the lower side of the chamber were incubated with crystal violet. The results were counted in three fields randomly selected by a forward microscope (Ni-V, Nikon, Japan). The data were extracted from three technical replicates.

Immunofluorometric assay

First, the treated cells on the round coverslip were fixed with 4% paraformaldehyde for 20 min, penetrated with 0.3% Triton X-100 for 15 min, incubated in a 5% BSA blocking buffer for 2 h at room temperature and then incubated with Vimentin and Cytokeratin-18 antibody (1:200 dilution) overnight at 4 ℃. The next day, secondary antibodies labeled with fluorescence (Alexa Fluor 488, Beyotime, 1:1,000) were applied for 1h at room temperature protected from light, followed by incubation with 0.1% DAPI for 10 min. Addition, cells were washed with PBS between each step. Finally, the cells were observed using a forward fluorescence microscope (Ni-V, Nikon, Japan), and photographs were recorded.

Statistical analysis

Statistical analysis was performed using SPSS 21.0 software. All the experimental results were expressed as mean ± standard deviation (SD). The Student's *t*-test was used to analyze the statistical difference between the experimental

and control groups. Moreover, the difference among multiple groups was determined by the one-way analysis of variance (ANOVA) test followed Turkey's posttest. P value <0.05 was considered significant.

Results

Screening of bioactive ingredients and putative targets from HJT

Forty-nine compounds of HJT were found in the literature, and all compounds were identified in the SwissADME database after applying the criteria of lipinski. The molecular names, structures and ADME-related parameters of these compounds are listed in *Table 1*. Finally, 36 bioactive compounds were screened from HJT, including 10 in Organic acids, 4 in Phenylethanoids, 5 in Phenylpropanoids, 1 in Flavonoid glycosides, 5 in Monoterpene glycosides, 7 in Octyl glycosides and 4 in other compounds.

According to the target screening of the bioactive compounds in the Chemmaper, Sea and Swiss database, 1,044 potential target genes were selected for the 36 compounds of HJT after removing duplicate targets (Table S1). Moreover, the UniProt database was used to translate the official names of potential targets so that they could be used in network construction for further biological characterization.

Construction of a compound-putative target network of HJT

Chinese herbal compounds can interfere with diseases by regulating a network through binding multiple targets. Therefore, a network of "compound-putative target" was established to predict these targets through the acquisition of detailed information on the bioactive ingredients of HJT. This network consisted of 969 nodes and 3,188 edges (*Figure 2A*), indicating the interactions of chemical compounds and putative targets. As can be seen from the figure, different active compounds corresponded to different targets, which reflected the characteristics of multi-compound, multi-target of HJT. Among them, the degree values of C-C8 (p-Coumaric acid), A-C9 (Ethyl gallate), C-C4((7R,8R)-3-Methoxy-8'-carboxy-7'-en-3',8-epoxy-7,4'-oxyneolignan-4,9-diol), A-C7 (4-Hydroxyphenylacetic acid), C-C10 (6-Feruloyloxyhexanoic acid), A-C3 (Vanillic acid β-glucoside) are the highest, 245, 223, 173, 166, 140 and 121 respectively, which indicated that they were the most

important active compounds in the network (*Figure 2B*).

Identification of TIF-related DEGs

Differential genetic analysis between TIF and healthy individuals was performed with |log2 FC| >1 and P<0.01. Ultimately, 1,283 DEGs were identified. A volcano plot of the distribution of DEGs is shown in *Figure 2C*. Among them, 580 up-regulated genes are represented by red dots, and 703 down-regulated genes are represented by green dots.

Analyses of enrichment of the KEGG pathway

As shown in *Figure 3A*, HJT has 79 genes that act on TIF. *Table 2* lists the specific details. The 79 cross gene were mapped to 218 pathways by KEGG enrichment analysis, the main signaling pathways involved in the treatment of TIF were identified and the first 25 pathways related to TIF and significantly enriched screened were screened (FDR <0.05) (*Table 3*), including Metabolic pathways (ko01100), Pathways in cancer (ko05200), MicroRNAs in cancer (ko05206), Relaxin signaling pathway (ko04926) among others. As the *Figure 3B* shown, the y-axis represents the KEGG pathway and the x-axis indicates the number of genes enriched in that pathway. The redder the color, the smaller the value of P_{adjust}; it also denotes greater credibility and greater importance. In contrast, the bluer the color, the greater the value of P_{adjust}. Addition, as shown in *Figure 3C*, enrichment of the KEGG pathway could be divided approximately into energy metabolism, environmental information processing, cellular process, organismal systems and human diseases. It is worth noting that the most genes are enriched in metabolic pathways (ko01100). This pathway contains a total of 1,554 genes, of which 24 of the above-mentioned 79 cross genes are included. And it contains 7 up-regulated genes and 17 down-regulated genes.

PPI network and co-expression network construction and analysis

The 79 cross genes were imported into STRING and the PPI network was obtained of which contains 65 nodes and 132 edges (*Figure 4A*). Subsequently, the topological properties of the afore-mentioned merged PPI network were analyzed according to three key parameters: BC, CC, and DC, screened targets above median values of BC,

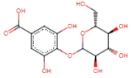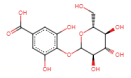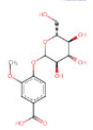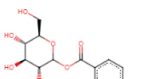**Table 1** Information for candidate bioactive compounds of HJT
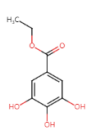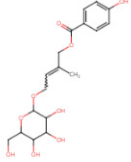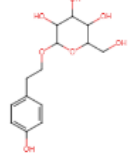
Category	Code name	Structure	Molecule name	Molecular formula	Lipinski	Molecular weight	Num. rotatable bonds	Num. H-bond acceptors	Num. H-bond donors
Organic acids	A-C1		4-(β-D-Glucopyranosyloxy)-3,5-dihydro xybenzoic acid or its isomer	C13H16O10	Yes; 1 violation: NHorOH >5	332.26 g/moL	4	10	7
	A-C2		4-(β-D-Glucopyranosyloxy)-3,5-dihydro xybenzoic acid or its isomer	C13H16O10	Yes; 1 violation: NHorOH >5	332.26 g/moL	4	10	7
	A-C3		Vanillic acid β-glucoside	C14H18O9	Yes; 0 violation	330.29 g/moL	5	9	5
	A-C4		Gallic acid	C7H6O5	Yes; 0 violation	170.12 g/moL	1	5	4
	A-C5		Protocatechuic acid	C7H6O4	Yes; 0 violation	154.12 g/moL	1	4	3
	A-C6		4-Hydroxybenzoic acid	C7H6O3	Yes; 0 violation	138.12 g/moL	1	3	2
	A-C7		4-Hydroxyphenylacetic acid	C8H8O3	Yes; 0 violation	152.15 g/moL	2	3	2
	A-C8		p-Hydroxybenzoic acid β-glucoside	C13H16O8	Yes; 0 violation	300.26 g/moL	4	8	5
	A-C9		Ethyl gallate	C9H10O5	Yes; 0 violation	198.17 g/moL	3	5	3
	A-C10		Creoside III	C18H24O9	Yes; 0 violation	384.38 g/moL	8	9	5
Phenylethanoids	B-C1		Salidroside	C14H20O7	Yes; 0 violation	300.30 g/moL	5	7	5

Table 1 *(continued)*
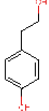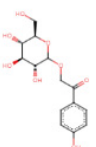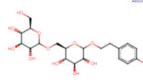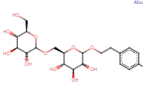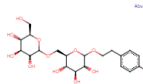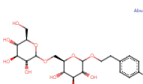
Page 8 of 23

Sun et al. Mechanisms and targets of HJT on TGFβ1-induced HK-2 cells
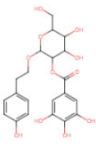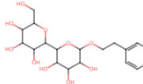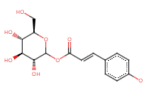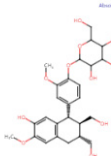
Table 1 *(continued)*

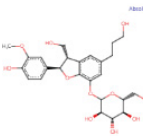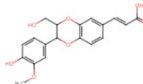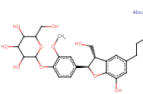| Category	Code name	Structure	Molecule name	Molecular formula	Lipinski	Molecular weight	Num. rotatable bonds	Num. H-bond acceptors	Num. H-bond donors
	B-C2		p-Tyrosol	C8H10O2	Yes; 0 violation	138.16 g/moL	2	2	2
	B-C3		2-(β-D-Glucopyranosyloxy)-1-(4-hydrox yphenyl) ethanone	C14H18O8	Yes; 0 violation	314.29 g/moL	5	8	5
	B-C4		2-(4-Hydroxyphenyl)-ethyl-O-β-D-gluco pyranosyl-6-O-β-D-glucopyranoside or its isomer	C20H30O12	No; 2 violations: NorO >10, NHorOH >5	462.45 g/moL	8	12	8
	B-C5		2-(4-Hydroxyphenyl)-ethyl-O-β-D-gluco pyranosyl-6-O-β-D-glucopyranoside or its isomer	C20H30O12	No; 2 violations: NorO >10, NHorOH >5	462.45 g/moL	8	12	8
	B-C6		2-(4-Hydroxyphenyl)-ethyl-O-β-D-gluco pyranosyl-6-O-β-D-glucopyranoside	C20H30O12	No; 2 violations: NorO >10, NHorOH >5	462.45 g/moL	8	12	8
	B-C7		2-(4-Hydroxyphenyl)-ethyl-O-β-D-gluco pyranosyl-6-O-β-D-glucopyranoside or its isomer	C20H30O12	No; 2 violations: NorO >10, NHorOH >5	462.45 g/moL	8	12	8
	B-C8		6"-O-Galloyl-salidroside	C21H24O11	No; 2 violations: NorO >10, NHorOH >5	452.41 g/moL	8	11	7
	B-C9		2-Phenylethyl-6-O-α-L-arabinopyranosyl-β-D-glucopyranoside	C19H28O10	Yes; 1 violation: NHorOH >5	416.42 g/moL	6	10	7
Phenylpropanoids	C-C1		1-O-p-Coumaroyl-β-D-glucopyranose	C15H18O8	Yes; 0 violation	326.30 g/moL	5	8	5
	C-C2		Lariciresinol-4-O-β-D-glucopyranoside	C26H34O11	No; 3 violations: MW >500, NorO >10, NHorOH >5	522.54 g/moL	8	11	7

Table 1 *(continued)*
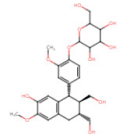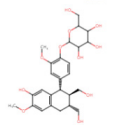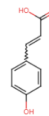
Table 1 *(continued)*

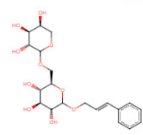| Category	Code name	Structure	Molecule name	Molecular formula	Lipinski	Molecular weight	Num. rotatable bonds	Num. H-bond acceptors	Num. H-bond donors
	C-C3		(7R,8S)-Dihydrodehydrodiconiferyl-alco hol-3'-O-β-D-glucopyranoside or (7R,8S)-Dihydrodehydrodiconiferyl-alco	C25H32O11	No; 3 violations: MW >500, NorO >10, NHorOH >5	508.51 g/moL	9	11	7
	C-C4		(7R,8R)-3-Methoxy-8'-carboxy-7'-en-3',8-epoxy-7,4'-oxyneolignan-4,9-diol	C19H18O7	Yes; 0 violation	358.34 g/moL	5	7	3
	C-C5		(7R,8S)-Dihydrodehydrodiconiferyl-alco hol-4-O-β-D-glucopyranoside	C25H32O11	No; 3 violations: MW >500, NorO >10, NHorOH >5	508.51 g/moL	9	11	7
	C-C6		Lariciresinol-4-O-β-D-glucopyranoside	C26H34O11	No; 3 violations: MW >500, NorO >10, NHorOH >5	522.54 g/moL	8	11	7
	C-C7		(+)-Isolarisiresinol-4-O-β-D-glucopyranoside	C26H34O11	No; 3 violations: MW >500, NorO >10, NHorOH >5	522.54 g/moL	8	11	7
	C-C8		p-Coumaric acid	C9H8O3	Yes; 0 violation	164.16 g/moL	2	3	2
	C-C9		Cinnamylalcohol-9-O-(6'-O-α-L-arabinopyranosyl)-β-D-glucopyranoside	C20H28O10	Yes; 1 violation: NHorOH >5	428.43 g/moL	7	10	6
	C-C10		6-Feruloyloxyhexanoic acid	C16H20O6	Yes; 0 violation	308.33 g/moL	10	6	2
Flavonoid glycosides	D-C1		Rhodionidin	C27H30O16	No; 3 violations: MW >500, NorO >10, NHorOH >5	610.52 g/moL	6	16	10
	D-C2		Kaempferol-7-rhamnoside	C21H20O10	Yes; 1 violation: NHorOH >5	432.38 g/moL	3	10	6

Table 1 *(continued)*
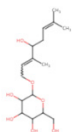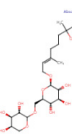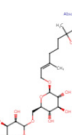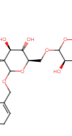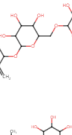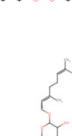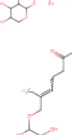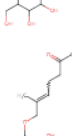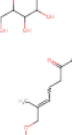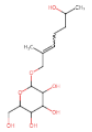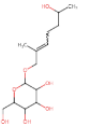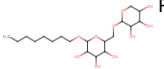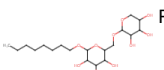
Page 10 of 23

Sun et al. Mechanisms and targets of HJT on TGFβ1-induced HK-2 cells

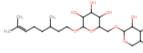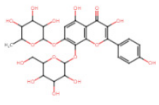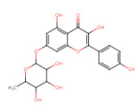**Table 1** *(continued)*

Category	Code name	Structure	Molecule name	Molecular formula	Lipinski	Molecular weight	Num. rotatable bonds	Num. H-bond acceptors	Num. H-bond donors
Monoterpene glycosides	E-C1		Rosiridin	C16H28O7	Yes; 0 violation	332.39 g/moL	7	7	5
	E-C2		Sachaloside VII	C21H38O11	No; 2 violations: NorO >10, NHorOH >5	466.52 g/moL	10	11	7
	E-C3		Sachaloside VIII	C21H38O11	No; 2 violations: NorO >10, NHorOH >5	466.52 g/moL	10	11	7
	E-C4		Sacranoside A	C21H34O10	Yes; 1 violation: NHorOH >5	446.49 g/moL	6	10	6
	E-C5		Sachaloside II	C21H34O10	Yes; 1 violation: NHorOH >5	446.49 g/moL	5	10	6
	E-C6		Creoside V	C21H38O10	Yes; 1 violation: NHorOH >5	450.52 g/moL	10	10	6
	E-C7		Kenposide A	C21H36O10	Yes; 1 violation: NHorOH >5	448.50 g/moL	9	10	6
Octylglycosides	F-C1		Creoside I	C14H24O7	Yes; 0 violation	304.34 g/moL	7	7	4
	F-C2		Creoside I	C14H24O7	Yes; 0 violation	304.34 g/moL	7	7	4
	F-C3		Creoside I	C14H24O7	Yes; 0 violation	304.34 g/moL	7	7	4

Table 1 *(continued)*

Table 1 *(continued)*

Category	Code name	Structure	Molecule name	Molecular formula	Lipinski	Molecular weight	Num. rotatable bonds	Num. H-bond acceptors	Num. H-bond donors
	F-C4		Creoside II	C14H26O7	Yes; 0 violation	306.35 g/moL	7	7	5
	F-C5		Creoside II	C14H26O7	Yes; 0 violation	306.35 g/moL	7	7	5
	F-C6		Rhodiooctanoside	C19H36O10	Yes; 1 violation: NHorOH >5	424.48 g/moL	11	10	6
	F-C7		Rhodiooctanoside	C19H36O10	Yes; 1 violation: NHorOH >5	424.48 g/moL	11	10	6
Other compounds	G-C1		4-Hydroxybenzyl-β-D-glucopyranoside	C13H18O7	Yes; 0 violation	286.28 g/moL	4	7	5
	G-C2		Picein	C14H18O7	Yes; 0 violation	298.29 g/moL	4	7	4
	G-C3		Creoside IV	C17H32O10	Yes; 1 violation: NHorOH >5	396.43 g/moL	9	10	6
	G-C4		Pyrogallol	C6H6O3	Yes; 0 violation	126.11 g/moL	0	3	3

HJT, Hongjingtian injection;

CC, and DC, thereby selecting the core genes of the TIF-treated effect of HJT. The cutoff value of the screening was BC >0.015, CC >0.304 and DC >3. These 25 core genes are marked in pink. Besides, the heat map of these 25 core genes were listed in *Figures 4B*. Finally, as shown in the *Figure 4C*, co-expression relationships in the PPI network were analyzed and further higher-scoring cluster containing 25 genes were shown in purple. Through the Venn diagram we found that there are 5 key genes enriched in the Metabolic pathway (ko01100), which were AKR1B1 (log2fc =−1.341623), GAD1 (log2fc =−1.563923), P4HA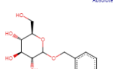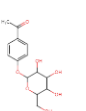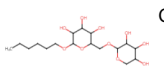2 (log2fc =1.069761), SPHK1 (log2fc =2.22411) and PTGES (log2fc =−2.268903). And there were three intersections between these five genes and the sub-network genes of

the co-expression network, *SPHK1*, *AKR1B* and *PTGES*, respectively. These results illustrate that *AKR1B1*, *GAD1*, *P4HA2*, *SPHK1* and *PTGES* may be key genes in HJT to regulate TIF through metabolic pathway, and there may be a co-expression relationship among *SPHK1*, *AKR1B1* and *PTGES*.

TGF affects the expression of AKR1B1, GAD1, P4HA2, SPHK1 and PTGES

We chose TGF-β1 to represent the severity of EMT *in vitro* cell models. In the above network pharmacological analysis, we predicted that *AKR1B1*, *GAD1*, *P4HA2*, *SPHK1* and *PTGES* in the metabolic pathway were key

Page 12 of 23

Sun et al. Mechanisms and targets of HJT on TGFβ1-induced HK-2 cells
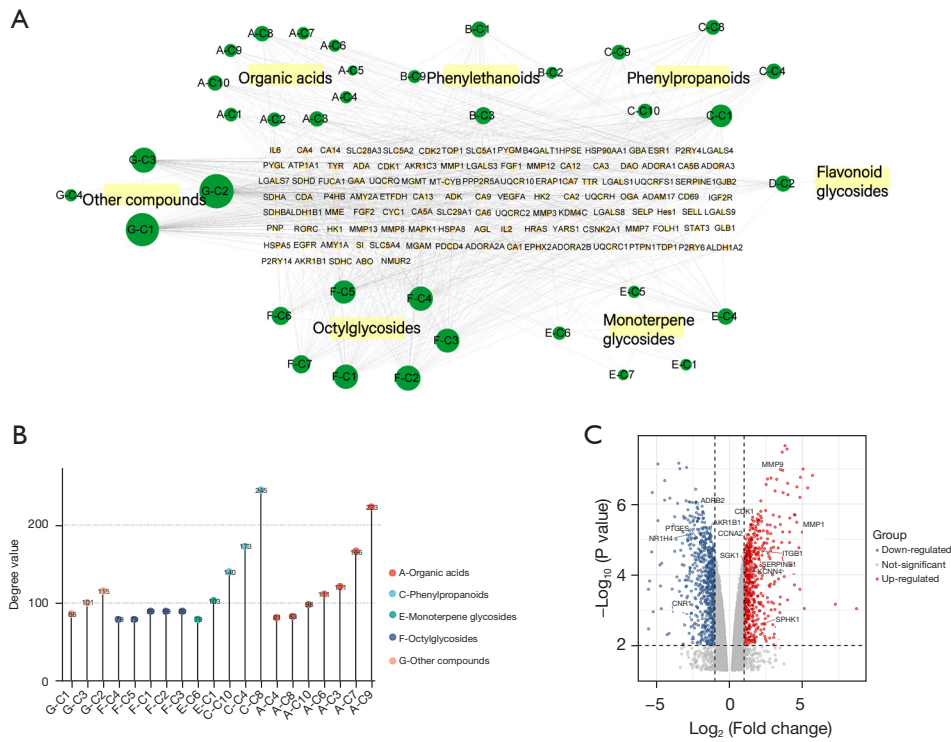
Figure 2 The information of HJT and GSE20247. (A) The compound-target network. The green nodes represent active compounds and the yellow nodes represent potential protein targets. The edges represent the interactions between them and nodes size are proportional to their degree. (B) Top 20 active compounds with degree value. (C) A volcano plot of the distribution of DEGs. HJT, Hongjingtian injection; DEG, differentially expressed gene.
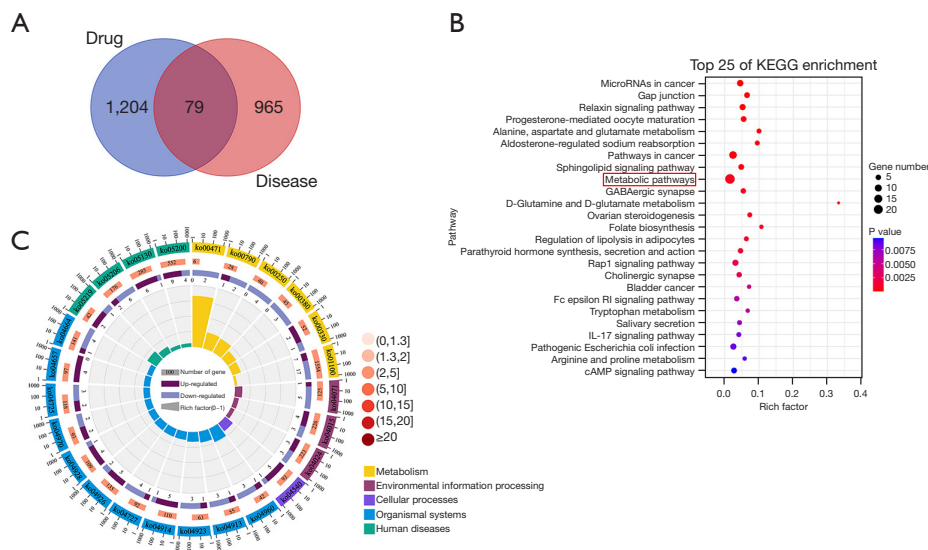
Figure 3 KEGG analysis. (A) 79 overlapping gene symbols between the disease and drug. (B) Top 25 pathways of KEGG enrichment. The y-axis represents the KEGG pathway and the x-axis indicates the number of genes enriched in that pathway. (C) Classification of 25 pathways. KEGG, Kyoto Encyclopedia of Genes and Genomes.

Table 2 Targets of HJT on TIF

Cross gene	Uniport ID	Gene name	LogFC
AKR1B1	P15121	Aldo-keto reductase family 1 member B	−1.34162
LGALS3	P17931	Lectin, galactoside binding soluble 3	1.333141
SERPINE1	P05121	Serpin family E member 1	1.977738
TNNC1	P63316	Troponin C1, slow skeletal and cardiac type	−2.18454
SCNN1A	P37088	Sodium channel epithelial 1 alpha subunit	−5.33779
DPP4	P27487	Dipeptidyl peptidase 4	−1.40641
AKR1C3	P42330	Aldo-keto reductase family 1, member C3	−1.09751
ADORA1	P30542	Adenosine A1 receptor	−1.54902
LPAR5	Q9H1C0	Lysophosphatidic acid receptor 5	4.496225
LPAR1	Q92633	Lysophosphatidic acid receptor 1	1.209421
P2RY2	P41231	Purinergic receptor P2Y2	1.40659
ADRB2	P07550	Adrenoceptor beta 2	−2.16687
P4HA1	P13674	Prolyl 4-hydroxylase subunit alpha 1	1.805188
IGFBP6	P24592	Insulin like growth factor binding protein 6	−1.61997
HMGB1	P09429	High mobility group box 1	1.269433
IGFBP5	P24593	Insulin like growth factor binding protein 5	−2.56708
GLRB	P48167	Glycine receptor beta	−1.04807
ALOX5	P09917	Arachidonate 5-lipoxygenase	−1.54864
PDE5A	O76074	Phosphodiesterase 5A	−2.85102
MMP9	P14780	Matrix metallopeptidase 9	3.495904
PIK3R1	P27986	Phosphoinositide-3-kinase regulatory subunit 1	−1.85214
KYNU	Q16719	Kynureninase	−1.20742
PHYKPL	Q8IUZ5	5-phosphohydroxy-L-lysine phospho-lyase	−1.01669
GAD1	Q8IVA8	Glutamate decarboxylase 1	−1.56392
SPTLC3	Q9NUV7	Serine palmitoyltransferase long chain base subunit 3	−1.72677
FYN	P06241	FYN proto-oncogene, Src family tyrosine kinase	−1.33082
CCNA2	P20248	Cyclin A2	1.395132
CDK1	P06493	Cyclin dependent kinase 1	1.591329
CCNB1	P14635	Cyclin B1	1.153017
MMP1	P03956	Matrix metallopeptidase 1	5.315018
MMP13	P45452	Matrix metallopeptidase 13	4.410247
PRKCA	P17252	Protein kinase C alpha	−1.28924
GATM	P50440	Glycine amidinotransferase	−1.26205
SLC23A1	Q9UHI7	Solute carrier family 23 member 1	−1.71022
PLOD2	O00469	Procollagen-lysine,2-oxoglutarate 5-dioxygenase 2	1.70937

Table 2 *(continued)*

Page 14 of 23

Sun et al. Mechanisms and targets of HJT on TGFβ1-induced HK-2 cells

Table 2 *(continued)*

Cross gene	Uniport ID	Gene name	LogFC
EGLN3	Q9H6Z9	Egl-9 family hypoxia inducible factor 3	−1.53998
P4HA2	O15460	Prolyl 4-hydroxylase subunit alpha 2	1.069761
SUCNR1	Q9BXA5	Succinate receptor 1	4.608116
ALDH5A1	P51649	Aldehyde dehydrogenase 5 family member A1	−1.95489
ENPEP	Q07075	Glutamyl aminopeptidase	−1.45376
GLS2	Q9UI32	Glutaminase 2	−1.03821
FPGS	Q05932	Folylpolyglutamate synthase	1.304325
GLS	O94925	Glutaminase	−1.27648
NR1H4	Q96RI1	Nuclear receptor subfamily 1 group H member 4	−2.90611
KMO	O15229	Kynurenine 3-monooxygenase (kynurenine 3-hydroxylase)	−3.60623
ESRRG	P62508	Estrogen related receptor gamma	−2.40246
PTGES	O14684	Prostaglandin E synthase	−2.2689
C3	P01024	Complement component 3	−1.83543
CYP26A1	O43174	Cytochrome P450 family 26 subfamily A member 1	−1.25634
KCNN4	O15554	Potassium calcium-activated channel subfamily N member 4	1.292726
Cyp24a1	Q07973	Cytochrome P450 family 24 subfamily A member 1	1.962299
ABCB1	P08183	ATP binding cassette subfamily B member 1	−2.63786
CNR1	P21554	Cannabinoid receptor 1	−2.36452
FOLR1	P15328	Folate receptor 1	−1.27459
ITGB1	P05556	Integrin subunit beta 1	2.271656
CYP1B1	Q16678	Cytochrome P450 family 1 subfamily B member 1	−1.12467
FOS	P01100	Fos proto-oncogene, AP-1 transcription factor subunit	1.069912
KCNK2	O95069	Potassium two pore domain channel subfamily K member 2	−2.09549
Hes1	Q14469	Hes family bHLH transcription factor 1	2.510727
SPHK1	Q9NYA1	Sphingosine kinase 1	2.22411
AURKB	Q96GD4	Aurora kinase B	1.554256
NEK2	P51955	NIMA related kinase 2	1.494727
TUBB4B	P68371	Tubulin beta 4B class IVb	1.123177
GPR183	P32249	G protein-coupled receptor 183	3.13216
TGM2	P21980	Transglutaminase 2	2.387535
TUBA4A	P68366	Tubulin alpha 4a	1.838797
XDH	P47989	Xanthine dehydrogenase	2.158727
CA11	O75493	Carbonic anhydrase 11	−1.2726
PRKACA	P17612	Protein kinase cAMP-activated catalytic subunit alpha	1.079271

Table 2 *(continued)*

Table 2 *(continued)*

Cross gene	Uniport ID	Gene name	LogFC
SCN2A	Q99250	Sodium voltage-gated channel alpha subunit 2	−1.45842
EIF4H	Q15056	Eukaryotic translation initiation factor 4H	1.779768
Sgk1	O00141	Serum/glucocorticoid regulated kinase 1	1.012613
DAPK1	P53355	Death associated protein kinase 1	−1.94583
Slc16a7	O60669	Solute carrier family 16 member 7	−1.38307
ST6GAL1	P15907	ST6 beta-galactoside alpha-2,6-sialyltransferase 1	−1.02237
AURKA	O14965	Aurora kinase A	1.16167
LSS	P48449	Lanosterol synthase (2,3-oxidosqualene-lanosterol cyclase)	−1.00177
Lat	O43561	Linker for activation of T-cells	1.492451
FKBP1A	P62942	FK506 binding protein 1A	1.071867

HJT, Hongjingtian injection; TIF, tubulointerstitial fibrosis; FC, fold change.

targets of HJT anti TIF. Thus, we chose these five key genes for further experimental verification. HK-2 cells were pretreated with TGF-β1 (0, 2, 5, 10 ng/mL) for 48 hours. Real-time polymerase chain reaction analysis results showed that compared with the control group (no TGF-β1 pre-treatment), *AKR1B1*, *GAD1*, *PTGES* were down-regulated and *SPHK1* and *P4HA2* were up-regulated by treatment of 10 ng/mL TGF-β1 in HK-2 cells (*Figure 5*).

These results are consistent with the expression trend of the microarray we explored. Finally, we selected TGF-β1 at 10 ng/mL to further investigate its effects on HJT to the expression of predicted five major gene targets based on the fact that none of the three concentrations of TGF-β1 inhibited cell activity.

Optimal concentration of HJT

It cannot be ignored that although HJT has a protective effect on HK-2 cells, high dose may cause cell death. In order to explore protective effects of HJT on the HK-2 cells, CCK-8 assay was used to evaluate the survival rate of HK-2 at the doses of 0, 1.25, 2.5, 5, 10, 20, 40, 80, 200, 1,000 mL/L of HJT. As the results showed in *Figure 6* that the HJT at the dose within the range of 0–2.5 mL/L has little significant toxicity in HK-2 cell. The half-maximal inhibitory concentration (IC50) of HJT for HK-2 cells was 99.81 mL/L. Therefore, 2.5 mL/L HJT was selected for subsequent experiments.

Effect of HJT on the expression of key targets in TGF-β1-induced HK-2

qRT-PCR was used to further validate *SPHK1*, *GAD1*, *P4HA2*, *AKR1B1* and *PTGES* for HJT treatment of TIF (*Figure 7A*). The results showed that HJT could reverse the expression of *SPHK1* with statistical significance (P<0.05). However, the improvement of other genes was not significant (P>0.05). The WB results demonstrated that the expression level of *SPHK1* was promoted in HK-2 (P<0.01). After treatment of HJT, the expression of *SPHK1* was markedly suppressed (P<0.05) (*Figure 7B,7C*).

The progression of EMT was promoted by TGF-β1 but restored by HJT

The immunofluorescence assay showed that TGF-β1 upregulated Vimentin and downregulated cytokeratin 18 in HK-2 cells. On the contrary, the expression of them was reversed after intervention with HJT (*Figure 8A,8B*). Besides, HK-2 migration capacity was measured through wound-healing assay and Transwell assay. As *Figure 8C,8D* shown, the first row was the scratch size of control, TGF-β1, HJT and TGF-β1 and HJT group at 0 h, which was used as a baseline comparison, while the second and third lines were the scratch size at 24 and 48 h in the corresponding groups, respectively. After 24 hours of intervention, TGF-β1 showed a 16.7% increase compared with control group

Page 16 of 23

Sun et al. Mechanisms and targets of HJT on TGFβ1-induced HK-2 cells

Table 3 Top 25 pathways

KEGG_A_class	KEGG_B_class	Pathway	Out [68]	All (8,312)	P value	Q value	Pathway ID
Human Diseases	Cancer: overview	MicroRNAs in cancer	8	176	0.000086	0.007876	ko05206
Cellular Processes	Cellular community-eukaryotes	Gap junction	6	93	0.000104	0.007876	ko04540
Organismal Systems	Endocrine system	Relaxin signaling pathway	7	135	0.000108	0.007876	ko04926
Organismal Systems	Endocrine system	Progesterone-mediated oocyte maturation	6	110	0.000263	0.013078	ko04914
Metabolism	Amino acid metabolism	Alanine, aspartate and glutamate metabolism	4	40	0.0003	0.013078	ko00250
Organismal Systems	Excretory system	Aldosterone-regulated sodium reabsorption	4	42	0.000363	0.013185	ko04960
Human Diseases	Cancer: overview	Pathways in cancer	13	552	0.00045	0.014012	ko05200
Environmental Information Processing	Signal transduction	Sphingolipid signaling pathway	6	125	0.000524	0.01428	ko04071
Metabolism	Global and overview maps	Metabolic pathways	24	1554	0.000866	0.018547	ko01100
Organismal Systems	Nervous system	GABAergic synapse	5	92	0.000896	0.018547	ko04727
Metabolism	Metabolism of other amino acids	D-Glutamine and D-glutamate metabolism	2	6	0.000969	0.018547	ko00471
Organismal Systems	Endocrine system	Ovarian steroidogenesis	4	55	0.001021	0.018547	ko04913
Metabolism	Metabolism of cofactors and vitamins	Folate biosynthesis	3	28	0.001482	0.024852	ko00790
Organismal Systems	Endocrine system	Regulation of lipolysis in adipocytes	4	63	0.001698	0.026438	ko04923
Organismal Systems	Endocrine system	Parathyroid hormone synthesis, secretion and action	5	109	0.001913	0.027803	ko04928
Environmental Information Processing	Signal transduction	Rap1 signaling pathway	7	226	0.002371	0.032308	ko04015
Organismal Systems	Nervous system	Cholinergic synapse	5	118	0.002708	0.034723	ko04725
Human Diseases	Cancer: specific types	Bladder cancer	3	42	0.004787	0.057971	ko05219
Organismal Systems	Immune system	Fc epsilon RI signaling pathway	5	141	0.005793	0.063375	ko04664
Metabolism	Amino acid metabolism	Tryptophan metabolism	3	45	0.005814	0.063375	ko00380
Organismal Systems	Digestive system	Salivary secretion	4	93	0.00693	0.071942	ko04970
Organismal Systems	Immune system	IL-17 signaling pathway	4	97	0.008026	0.078979	ko04657
Human Diseases	Infectious disease: bacterial	Pathogenic Escherichia coli infection	7	285	0.008397	0.078979	ko05130
Metabolism	Amino acid metabolism	Arginine and proline metabolism	3	52	0.008695	0.078979	ko00330
Environmental Information Processing	Signal transduction	cAMP signaling pathway	6	223	0.009555	0.082423	ko04024

KEGG, Kyoto Encyclopedia of Genes and Genomes; RI, receptor for immunoglobulin E; cAMP, cyclic adenosine monophosphate.
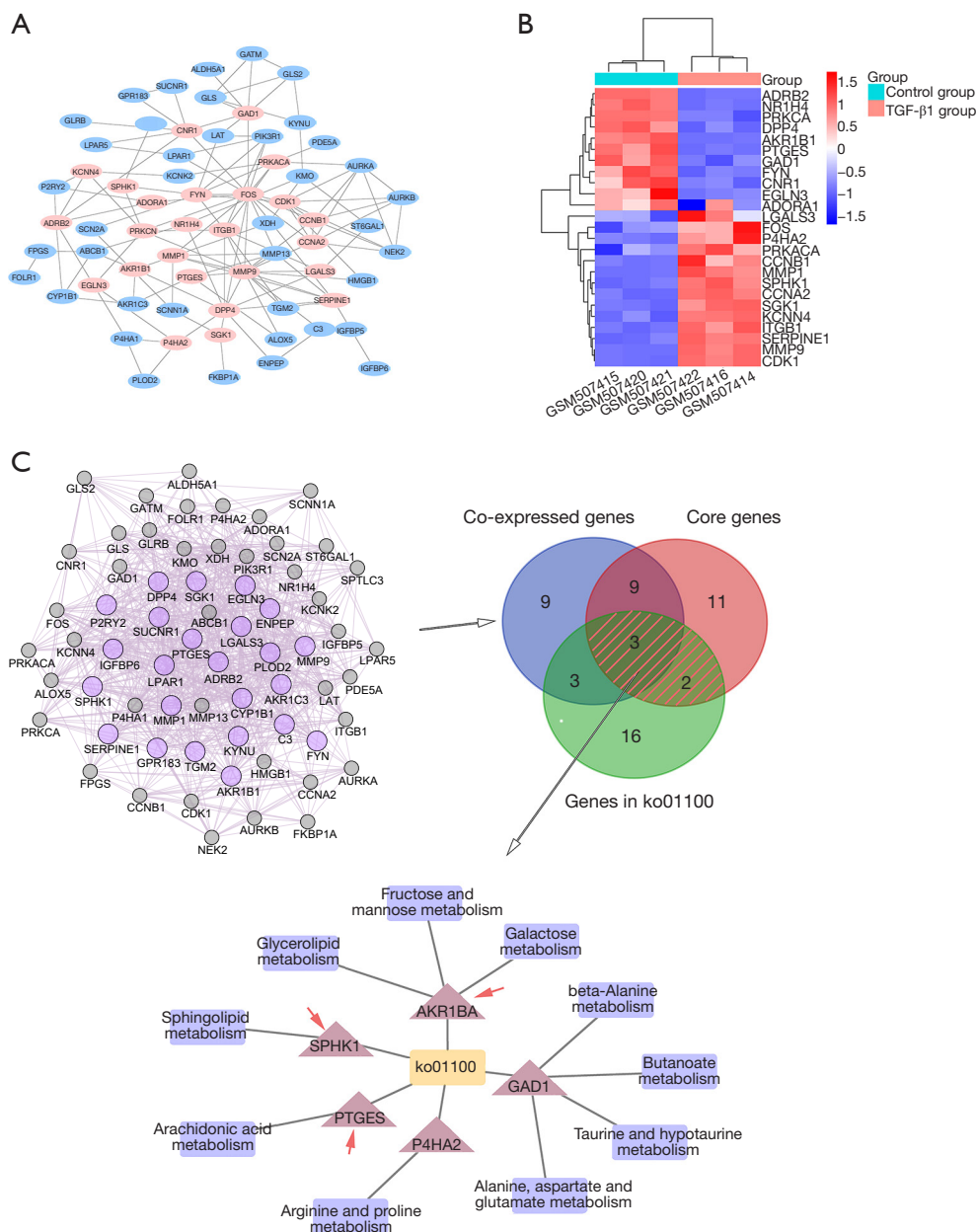
Figure 4 Analysis of PPI and key genes. (A) Protein-protein interaction network of HJT acting on TIF. Network nodes represent proteins, edges represent protein-protein associations. The pink nodes represent 25 core genes. (B) The heatmap of core genes. (C) Co-expression relationships in the PPI network were analyzed and further higher-scoring cluster containing 25 genes were shown in purple. There are 5 key genes enriched in the Metabolic pathway, three of which have co-expression relationship, *SPHK1*, *AKR1B1* and *PTGES*, respectively. PPI, protein-protein interaction; HJT, Hongjingtian injection; TIF, Tubulointerstitial fibrosis.

(P<0.05), and 5.6% decrease of TGF-β1 + HJT to TGF-β1 (P>0.05). After 48 hours of intervention, TGF-β1 showed a 21.1% increase compared with control group (P<0.05), and 16.7% decrease of TGF-β1 + HJT to TGF-β1 (P<0.05).

To conform the effects on cells migration, Transwell assay was carried out and TGF-β1 showed a 550.2% increase in comparison with control group (P<0.0001). TGF-β1 + HJT showed a 44.9% decrease in comparison with TGF-β1

Page 18 of 23

Sun et al. Mechanisms and targets of HJT on TGFβ1-induced HK-2 cells
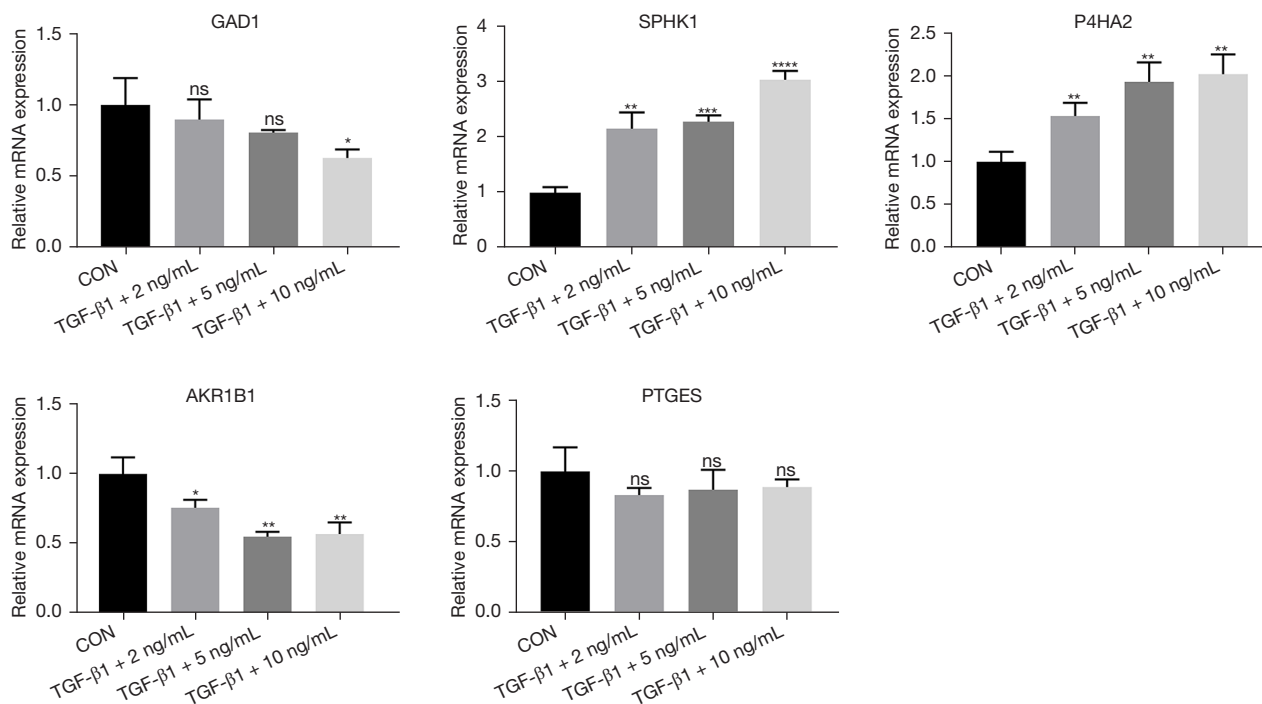

Figure 5 The effect of different concentrations of TGF-β1 on five key genes was determined by qPCR. *, P<0.05; **, P<0.01; ***, P<0.001; ****, P<0.0001; ns, P>0.05. CON, control group; qPCR, quantitative polymerase chain reaction.
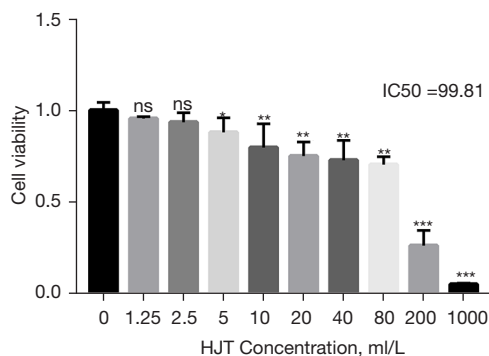

Figure 6 Evaluate the survival rate of HK-2 at the different doses of HJT using CCK-8 assay. *, P<0.05; **, P<0.01; ***, P<0.001; ns, P>0.05. HJT, Hongjingtian injection.

(P<0.0001, *Figure 8E,8F*). Taken together, TGF-β1 could regulate vimentin and cytokeratin 18, and promote the migration of HK-2 cells, consequently accelerated the EMT progression. However, HJT can reverse the phenomenon.

Discussion

TIF is a key and irreversible process in the development of CKD. Existing treatment strategies are insufficient to prevent disease development. Therefore, more effective treatments are needed to delay the progression of TIF. In recent years, traditional Chinese medicine has become popular in western countries due to its reliable efficacy. In TCM theory, TIF is called edema, strangury, consumptive disease and so on. Its pathological mechanism can be roughly summarized as deficiency, blood stasis, phlegm dampness and turbid toxin. Rhodiola, as one of the traditional Tibetan medicines in China, has long existed in the history of medicine. It has the effect of invigorating Qi and promoting blood circulation, clearing the pulse and relieving asthma. In modern pharmacology, Rhodiola has anti-diabetic, anti-inflammatory, anti-cancer, anti-aging, cardio-protective, and neuro-protective effects (12). However, as a preparation extracted from Rhodiola, the mechanism of HJT in treating TIF is still unclear due to the
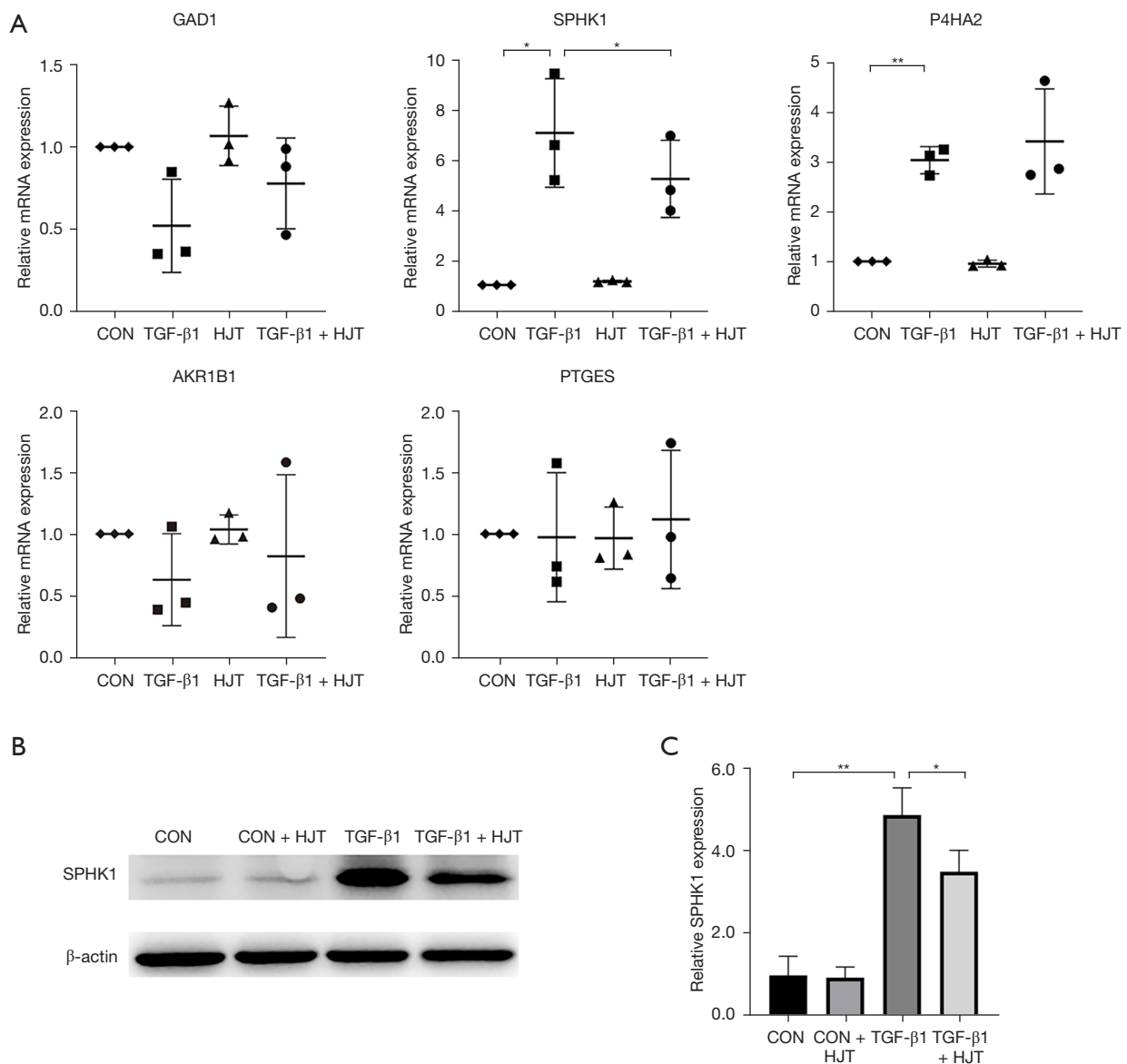
Figure 7 Effect of HJT on five key genes in HK-2 interfered by TGF-β1. (A) Effect of HJT on the expression of key targets in TGF-β1-induced HK-2. *, P<0.05. **, P<0.01. (B,C) The expression level of *SPHK1* was promoted in HK-2 (**, P<0.01). After the treatment of HJT, the expression of *SPHK1* was markedly suppressed (*, P<0.05). HJT, Hongjingtian injection.

complex compounds of traditional Chinese medicine. Thus, this study aimed to clarify the potential mechanism of HJT in the treatment of TIF based on network pharmacology.

We screened out 36 effective active compounds and 1,044 potential targets of HJT. Among the main active compounds of HJT, p-Coumaric acid (p-CA) is a phenolic acid of the hydroxycinnamic acid family (13). Extensive studies have shown that p-CA is related to various bioactivities, including antioxidant, anti-inflammatory, anti-

cancer and antidiabetic (14). Mani *et al.* has revealed that p-CA was found to offer renal protection from oxidative stress by decreasing lipid peroxidation and increasing the activities of antioxidant enzymes in treated diabetic rats (15). Zabad *et al.* also reported that P-CA are able to decrease the fibrotic cytokines and protect against the progression of DKD (16). Ethyl gallate (EG) is a hydroxylated, ethyl ester of benzoic acid. EG has antioxidant, anti-inflammatory and anti-proliferative effects. Cui *et al.* (17) demonstrated
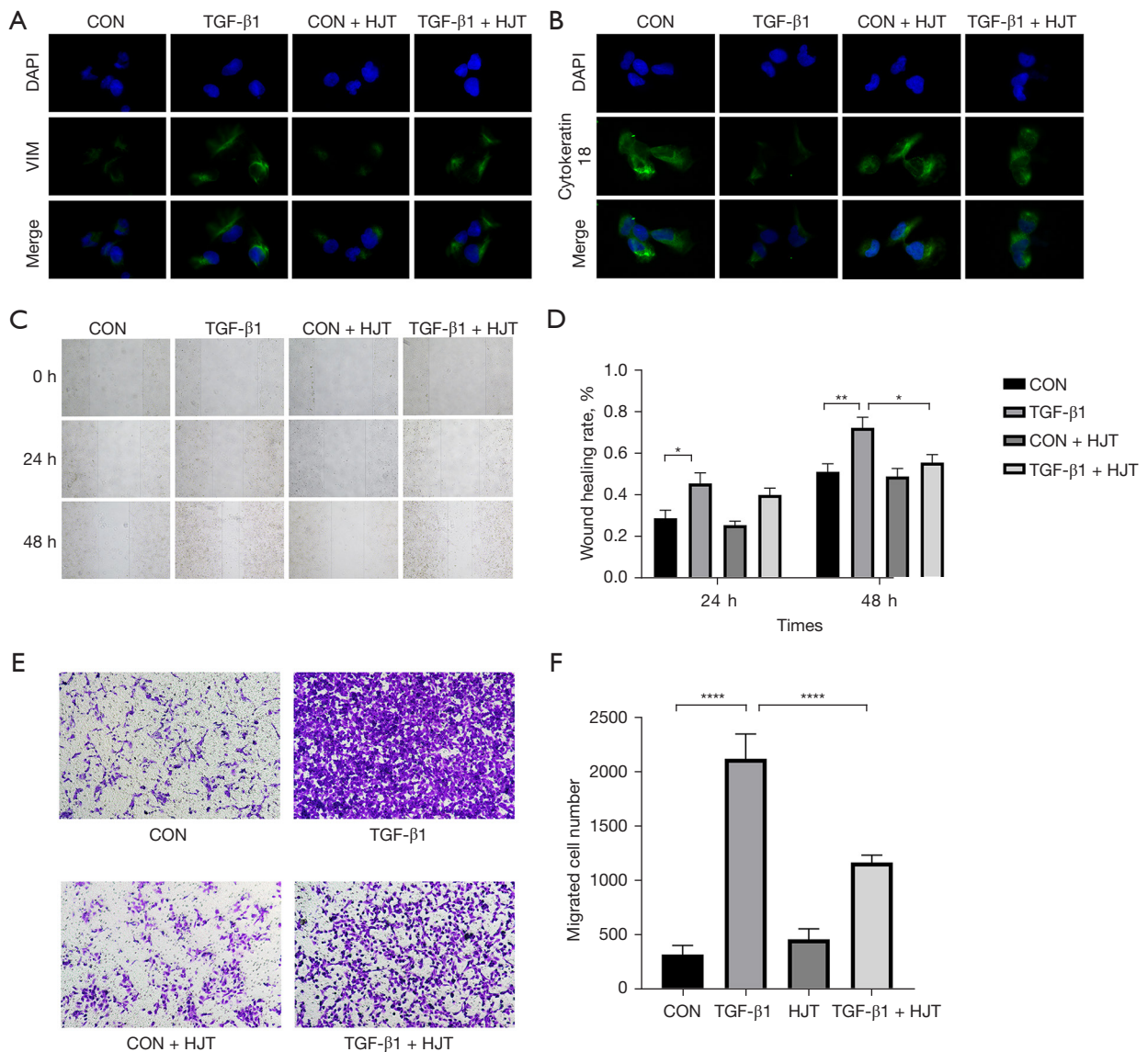
Ann Transl Med 2022;10(24):1329 | https://dx.doi.org/10.21037/atm-22-5035

Page 20 of 23

Sun et al. Mechanisms and targets of HJT on TGFβ1-induced HK-2 cells

Figure 8 The progression of EMT was promoted by TGF-β1 but restored by HJT. (A,B) The immunofluorescence assay showed that TGF-β1 upregulated Vimentin and downregulated cytokeratin18 in HK-2 cells. On the contrary, the expression of them was reversed after intervention with HJT. (40×). (C,D) Wound healing assay. The three lines were the scratch size at 0, 24 and 48 h in the corresponding groups, respectively (40×). (E,F) Transwell assay (Crystal violet stain, 40×). *, P<0.05. **, P<0.01. ****, P<0.0001. HJT, Hongjingtian injection. DAPI, 4',6-diamidino-2-phenylindole, a fluorescent dye with strong binding to DNA. VIM, Vimentin.

that EG suppresses proliferation and invasion in human breast cancer cells by modulating the *PI3K/Akt* pathway, and inhibit downstream targets such as *NF-κB p-65*, *Bcl-2/Bax*. Ahn *et al.* (18) proposed that EG targeting *PTPN6* and *PPARγ* exerts an anti-diabetes effect. Crispo *et al.* (19) suggested that EG protects PC12 cells against oxidative stress induction through the *Nrf2* pathway. As such, it

has been proved that EG can protect against diabetes, neuro-degenerative disease, endothelial inflammation and some types of cancer (20). In addition, both 4-Hydroxyphenylacetic acid 4 and Vanillic acid β-glucoside showed potential antioxidant effects (21,22).

Meanwhile, the GSE20247 dataset was downloaded from the GEO database to obtain the gene expression data

of TGF intervention HK-2 cells, and then analyzed the DEGs. In addition, PPI network and functional enrichment analysis were performed on common genes to understand the meaningful pathway between TGF-β1-induced HK-2 and normal control. Of which, Metabolic pathways is the pathway enriched for the most genes compared to other pathways. We speculated that HJT might participate in the treatment of TIF by regulating metabolic pathways. Therefore, five target genes related to metabolic pathways were selected for further research (*AKR1B1*, *GAD1*, *P4HA2*, *SPHK1* and *PTGES*).

Our result shows that although it was found that the five key genes in HK-2 interfered by TGF-β1 were consistent with the trend shown by the GSE20247, HJT only had a significant reversal effect on *SPHK1*. The metabolites of sphingolipid include ceramides, sphingosine and sphingosine-1-phosphate (S1P). S1P has a function of cell proliferation and differentiation, while ceramide and sphingosine induced cell growth arrest and apoptosis and migration (23). *SPHK1* is a key metabolic enzyme that catalyzes the synthesis of S1P by sphingosine (24). Fibronectin (FN) is one of ECM components and its accumulation will eventually lead to TIF (25). Chen *et al.* demonstrated that AGEs-RAGE could upregulate FN through regulating *SPHK1 in vitro* cell experiments (26). Huang *et al.* (27) confirmed the regulatory effect of *SPHK1* on *NF-κB*-mediated diabetic renal fibrosis *in vivo* and *in vitro* experiments. Compared with diabetic mice, fewer renal fibrotic lesions, FN accumulation and *NF-κB* nuclear accumulation exhibited in glomeruli of kidneys of *SPHK1*$^{-/-}$ diabetic mice. He *et al.* (28) indicated that the inhibition of *SPHK1* contribute to decrease the EMT by blocking the *NF-κB* signaling, thereby protecting HK-2 against TIF. Liu *et al.* (29) confirmed that *SPHK1*/S1P signaling upregulates microRNA-21 in renal TECs interfered by TGF-β, thus promoting the overexpression of ECM proteins and TIF. Huang *et al.* (30) reported that the expression of *SPHK1* and S1P were significantly down-regulated by curcumin in diabetic rat kidneys and glomerular mesangial cells (GMCs) with high glucose intervention. Meanwhile, *SPHK1*-S1P-mediated FN and TGF-β1 were inhibited. In addition, Lan *et al.* (31) also found that berberine exerts renoprotective effects on DKD through *SPHK1*–S1P signaling pathway. S1P is catalytically synthesized by Sphingosine kinases and catabolized by S1P phosphatases and S1P lyase (S1PL). Huang *et al.* (32) suggested that the expressions of *SPHK1* were increased in bleomycin challenged mice. Genetic knockdown of *SPHK1* ameliorated pulmonary fibrosis in

mice while deletion of S1PL potentiated fibrosis. Taken together, the present study *in vitro* and *in vivo* demonstrated that *SPHK1* is closely related to the pathological process of EMT and TIF. Therefore, inhibiting *SPHK1* signaling may be a promising therapeutic strategy in TIF.

During the process of TIF, epithelial cells undergo partial EMT. Partial EMT cells acquire the ability to produce profibrotic cytokines/growth factors while remaining attached to the basement membrane during fibrosis (33). In addition, a study (34) has found that compared with the normal structure of renal tubules in healthy subjects, renal sections of diabetes patients show thickening and hypertrophy of renal tubules. As a key mediator of TIF, TGF-β1 activates different intracellular signaling pathways during the process of EMT (35), contributing to the secretion of collagen and inducing its deposition, leading to tissue fibrosis (36). Besides, TGF-β1 is also closely related to hypertrophy of renal tubules (37). Therefore, we established an *in vitro* TIF cell model by intervening HK-2 cells with TGF-β1. During EMT, epithelial cells lose key phenotypic markers and acquire mesenchymal markers (38). In our results, it was clearly seen that HJT alone did not affect the migration and phenotypic changes of HK-2 without TGF-β1 intervention. The results of immunofluorescence showed that the expression of cytokeratin 18 decreased and the expression of vimentin increased after TGF-β1 intervention, and then reversed by HJT. In the wound healing assay and Transwell assay, compared with the control group, the TGF-β1 experimental group significantly improved the cell migration ability, but the ability decreased after adding HJT. To sum up, HJT has an inhibitory effect on EMT and migration ability. HJT treatment of TIF may reverse EMT caused by TGF-β1 by targeting *SPHK1*.

Conclusions

In conclusion, HJT treats TIF through multi-component, multi-target and multi-directional. In particular, SPHK1 may be the most important target of HJT in TIF. Our research revealed the mechanism of HJT in the process of action from a holistic and systematic perspective, which provides a theoretical basis for further research and application of HJT in the future. However, whether HJT is indeed suitable for the prevention and treatment of TIF still needs to be confirmed by future clinical trials. Therefore, *in vivo* experimental validation of potential active ingredients is urgently needed to help further evaluate the therapeutic potential of HJT.

Acknowledgments

Footnote

Reporting Checklist: The authors have completed the MDAR reporting checklist. Available at https://atm.amegroups. com/article/view/10.21037/atm-22-5035/rc

Data Sharing Statement: Available at https://atm.amegroups. com/article/view/10.21037/atm-22-5035/dss

Conflicts of Interest: All authors have completed the ICMJE uniform disclosure form (available at https://atm. amegroups.com/article/view/10.21037/atm-22-5035/coif). The authors have no conflicts of interest to declare.

Ethical Statement: The authors are accountable for all aspects of the work in ensuring that questions related to the accuracy or integrity of any part of the work are appropriately investigated and resolved. The study was conducted in accordance with the Declaration of Helsinki (as revised in 2013).

References

1. Webster AC, Nagler EV, Morton RL, et al. Chronic Kidney Disease. Lancet 2017;389:1238-52.

2. Djudjaj S, Boor P. Cellular and molecular mechanisms of kidney fibrosis. Mol Aspects Med 2019;65:16-36.

3. Zhang Z, Ma J, Feng R, et al. Centella asiatica inhibits renal interstitial fibrosis by regulating Smad3 and Smad7 expression in the TGFbeta signaling pathway. Int J Clin Exp Pathol 2018;11:1009-17.

4. Gu LY, Yun S, Tang HT, et al. Huangkui capsule in combination with metformin ameliorates diabetic nephropathy via the Klotho/TGF-beta1/p38MAPK signaling pathway. J Ethnopharmacol 2021;281:113548.

5. Li X, Chen S, Shao W. Effect of Hongjingtian injection on serum high-sensitivity C-reactive protein and degree of atherosclerosis in patients with essential hypertension. Shaanxi Journal of Traditional Chinese Medicine 2017;38:161-2.

6. Zhao J, Liu Y, Chen S. Effect of Hongjingtian injection on hemorheology in patients with type 2 diabetes mellitus. Clinical Journal of Chinese Medicine 2016;8:29-30.

7. Guo C, Li Y, Zhang R, et al. Protective Effect of Salidroside Against Diabetic Kidney Disease Through Inhibiting BIM-Mediated Apoptosis of Proximal Renal Tubular Cells in Rats. Front Pharmacol 2018;9:1433.

8. Liu Y, Chen C, Qiu J, et al. Characterization of the chemical constituents in Hongjingtian injection by liquid chromatography quadrupole time-of-flight mass spectrometry. Biomed Chromatogr 2019;33:e4446.

9. Kanehisa M, Goto S. KEGG: kyoto encyclopedia of genes and genomes. Nucleic Acids Res 2000;28:27-30.

10. Szklarczyk D, Morris JH, Cook H, et al. The STRING database in 2017: quality-controlled protein-protein association networks, made broadly accessible. Nucleic Acids Res 2017;45:D362-8.

11. Tang Y, Li M, Wang J, et al. CytoNCA: a cytoscape plugin for centrality analysis and evaluation of protein interaction networks. Biosystems 2015;127:67-72.

12. Lee Y, Jung JC, Jang S, et al. Anti-Inflammatory and Neuroprotective Effects of Constituents Isolated from Rhodiola rosea. Evid Based Complement Alternat Med 2013;2013:514049.

13. Cha H, Lee S, Lee JH, et al. Protective effects of p-coumaric acid against acetaminophen-induced hepatotoxicity in mice. Food Chem Toxicol 2018;121:131-9.

14. Amalan V, Vijayakumar N, Indumathi D, et al. Antidiabetic and antihyperlipidemic activity of p-coumaric acid in diabetic rats, role of pancreatic GLUT 2: In vivo approach. Biomed Pharmacother 2016;84:230-6.

15. Mani A, Kushwaha K, Khurana N, et al. p-Coumaric acid attenuates high-fat diet-induced oxidative stress and nephropathy in diabetic rats. J Anim Physiol Anim Nutr (Berl) 2022;106:872-80.

16. Zabad OM, Samra YA, Eissa LA. P-Coumaric acid alleviates experimental diabetic nephropathy through

modulation of Toll like receptor-4 in rats. Life Sci 2019;238:116965.

17. Cui H, Yuan J, Du X, et al. Ethyl gallate suppresses proliferation and invasion in human breast cancer cells via Akt-NF-kappaB signaling. Oncol Rep 2015;33:1284-90.

18. Ahn D, Kim J, Nam G, et al. Ethyl Gallate Dual-Targeting PTPN6 and PPARγ Shows Anti-Diabetic and Anti-Obese Effects. Int J Mol Sci 2022;23:5020.

19. Crispo JA, Piché M, Ansell DR, et al. Protective effects of methyl gallate on H2O2-induced apoptosis in PC12 cells. Biochem Biophys Res Commun 2010;393:773-8.

20. Wang HR, Sui HC, Ding YY, et al. Stimulation of the Production of Prostaglandin E2 by Ethyl Gallate, a Natural Phenolic Compound Richly Contained in Longan. Biomolecules 2018;8:91.

21. Zhao H, Jiang Z, Chang X, et al. 4-Hydroxyphenylacetic Acid Prevents Acute APAP-Induced Liver Injury by Increasing Phase II and Antioxidant Enzymes in Mice. Front Pharmacol 2018;9:653.

22. Kayano S, Kikuzaki H, Fukutsuka N, et al. Antioxidant activity of prune (Prunus domestica L.) constituents and a new synergist. J Agric Food Chem 2002;50:3708-12.

23. Takehara M, Bandou H, Kobayashi K, et al. Clostridium perfringens alpha-toxin specifically induces endothelial cell death by promoting ceramide-mediated apoptosis. Anaerobe Oct 2020;65:102262.

24. Pulkoski-Gross MJ, Obeid LM. Molecular mechanisms of regulation of sphingosine kinase 1. Biochim Biophys Acta Mol Cell Biol Lipids 2018;1863:1413-22.

25. Gong W, Chen C, Xiong F, et al. CKIP-1 ameliorates high glucose-induced expression of fibronectin and intercellular cell adhesion molecule-1 by activating the Nrf2/ARE pathway in glomerular mesangial cells. Biochem Pharmacol 2016;116:140-52.

26. Chen C, Gong W, Li C, et al. Sphingosine kinase 1 mediates AGEs-induced fibronectin upregulation in diabetic nephropathy. Oncotarget 2017;8:78660-76.

27. Huang J, Li J, Chen Z, et al. Sphingosine kinase 1 mediates diabetic renal fibrosis via NF-kappaB signaling pathway: involvement of CK2alpha. Oncotarget 2017;8:88988-

89004.

28. He F, Fan M, Jin Y, et al. Sphingosine kinase 1 inhibition decreases the epithelial-mesenchymal transition and ameliorates renal fibrosis via modulating NF-κB signaling. Am J Transl Res 2019;11:5879-87.

29. Liu X, Hong Q, Wang Z, et al. Transforming growth factor-β-sphingosine kinase 1/S1P signaling upregulates microRNA-21 to promote fibrosis in renal tubular epithelial cells. Exp Biol Med (Maywood) 2016;241:265-72.

30. Huang J, Huang K, Lan T, et al. Curcumin ameliorates diabetic nephropathy by inhibiting the activation of the SphK1-S1P signaling pathway. Mol Cell Endocrinol 2013;365:231-40.

31. Lan T, Shen X, Liu P, et al. Berberine ameliorates renal injury in diabetic C57BL/6 mice: Involvement of suppression of SphK-S1P signaling pathway. Arch Biochem Biophys 2010;502:112-20.

32. Huang LS, Natarajan V. Sphingolipids in pulmonary fibrosis. Adv Biol Regul 2015;57:55-63.

33. Grande MT, Sánchez-Laorden B, López-Blau C, et al. Snail1-induced partial epithelial-to-mesenchymal transition drives renal fibrosis in mice and can be targeted to reverse established disease. Nat Med 2015;21:989-97.

34. Habib SL. Alterations in tubular epithelial cells in diabetic nephropathy. J Nephrol 2013;26:865-9.

35. Sutariya B, Jhonsa D, Saraf MN. TGF-β: the connecting link between nephropathy and fibrosis. Immunopharmacol Immunotoxicol 2016;38:39-49.

36. Sekar V, Mani S, Malarvizhi R, et al. Positive interaction of mangiferin with selected oral hypoglycemic drugs: a therapeutic strategy to alleviate diabetic nephropathy in experimental rats. Mol Biol Rep 2020;47:4465-75.

37. Vallon V, Thomson SC. Renal function in diabetic disease models: the tubular system in the pathophysiology of the diabetic kidney. Annu Rev Physiol 2012;74:351-75.

38. Patel NA, Patel PS, Vora HH. Role of PRL-3, Snail, Cytokeratin and Vimentin expression in epithelial mesenchymal transition in breast carcinoma. Breast Dis 2015;35:113-27.